Supporting Information Appendix

De novo mutation in *RING1* with epigenetic effects on neurodevelopment

SI Results

Clinical characterization. The patient is the only child of healthy unrelated parents of European ancestry. Family histories of both parents are unremarkable. She was born at 40 weeks gestation with mild intrauterine growth retardation and microcephaly. Her birth weight was 1.96 kg (0.1 percentile, -3.2 SD), length was 43 cm (0.1 percentile, -4.2 SD), and head circumference was 30 cm (0.1 percentile, -4.9 SD). Bilateral hernias were repaired at 5 mo of age. Early motor and language development were normal. After the first year of life she showed delayed acquisition of additional language and cognitive skills and delayed adaptive social skills. At age 13 yr her weight was 31 kg (<1 percentile, -2.7 SD), height was 148.4 cm (<5 percentile, -1.8 SD), and head circumference was 49.1 cm (<1 percentile, -4.2 SD). Also at age 13 yr she developed a vasculitic-appearing rash on her lower extremities consistent with Henoch-Schönlein purpura, and bilateral flexion contractures of her fifth digits. Skeletal analysis indicated mild scoliosis of the lower thoracic and upper lumbar spine, without any gross bone abnormalities. Psychotic symptoms began at approximately age 13 yr, including hearing multiple voices, belief she was being poisoned, and confused disorganized thinking. Cognitive testing showed a verbal IQ of 55 and a visual performance IQ of 63. She receives special education services. Electroencephalography, brain magnetic resonance imaging, and brain computed tomography scans at age 13 yr were normal. Chromosome analysis at the 550-band level was normal.

SI Materials and Methods

Human subjects. The study was approved by the institutional review boards of the University of Washington (protocol 29501) and of Seattle Children's Hospital (protocol 11106). All subjects provided written informed consent.

Genomics. DNA was extracted from peripheral blood samples of the patient and her parents. Whole exomes were captured using VCRome v2.1 (NimbleGen) and then sequenced on a HiSeq 2500 (Illumina) at a mean target depth of 80X. More than 97% of targeted basepairs had >8 high-quality reads. Sequenced reads were aligned to hg19 using BWA (BWA-MEM v0.7.9a) and variants were called using GATK Unified Genotyper (3.0-0-g6bad1c6). Annotations, filtering, and variant prioritizations were conducted using in-house scripts as previously described (1). Rare variants were classified by genetic model and predicted function. Candidate variants were validated by PCR amplification and Sanger sequencing. Primers used for validation of *RING1* c.284G>A were 5'-cattcagaactcatgtgcccta-3' and 5'-ggatgctgaggcttagaagcta-3'.

Cloning and protein purification. Human cDNAs were purchased (GE Healthcare). The Gibson assembly method (2) was used to clone amino acids 1-113 of RING1 (NP_002922.2) downstream of a thrombin cleavable His_6-GST tag in a pGEX-4T vector (GE Healthcare) and to introduce the p.R95Q mutation. PCGF1 (amino acids 13-150, NP_116062.2) and BMI1 (amino acids 1-109, NP_005171.4) were cloned into pET28a vectors (Novagen) downstream of the His_6 tag. RING1 and either PCGF1 or BMI1 were co-expressed in Rosetta 2 *E. coli* cells (Novagen) in the presence of 150 μM $ZnCl_2$. Expression was induced at optical density 0.6 with 200 μM IPTG, overnight at 16°C. The complex was co-purified using a GSTrap column (GE Healthcare) according to the

manufacturer's protocol. The complex was then dialyzed against 25 mM sodium phosphate pH 7.0, 50 mM sodium chloride at 4ºC before storage at -80ºC. Wild-type and R95Q complexes produced similar yields, suggesting the mutation does not lead to loss of protein stability. Ub, HA-tagged Ub, E1 (Uba1) and E2 (Ube2d3) were expressed and purified as described previously (3, 4). Histones and 147 base pairs of double stranded DNA were purified and assembled into mononucleosomes as established previously (5).

Ubiquitylation assays. All *in vitro* assays were carried out in 25 mM sodium phosphate pH 7.0, 150 mM sodium chloride at 37ºC with shaking. To determine the ability of RING1 variants to enhance the formation of ubiquitin chains, assays were carried out using 20 μM HA-tagged Ub, 2.5 μM E1, 10 μM E2, 5 mM ATP, 5 mM $MgCl_2$, and 2.8 μM RING1/PCGF. Samples of the reaction were collected at 0, 2, 4, and 16 min and added to denaturing and reducing sample load dye to stop the ubiquitylation reaction. Samples were applied to 4-20% SDS-PAGE gradient gels (Bio-Rad), transferred to nitrocellulose for one hour at 100 volts, and immunoblotted with an antibody to the HA tag on Ub (Bethyl Laboratories, A190-108A; 1:5000). Nucleosome ubiquitylation was assayed with 20 μM Ub, 1 μM E1, 4 μM E2, 0.12 μM mononucleosomes, 5 mM ATP, 5 mM $MgCl_2$, and 4 μM of the specified RING1/PCGF heterodimeric pair. Samples were collected at 0, 20, and 60 min after ATP addition and added to denaturing and reducing sample load dye to stop the ubiquitylation reaction. Samples were applied to 15% gels, transferred to nitrocellulose for 1.5 hours at 100 volts, and immunoblotted with an antibody to the H2A acidic patch (EMD Millipore, 07-146; 1:1000). All western blots were imaged using an Odyssey infrared imaging system (Licor). Both ubiquitylation assays were repeated with independent protein and nucleosome preparations with similar results.

Protein structure visualization. Structures were visualized and cartoons rendered with the PyMOL Molecular Graphics System, version 1.8, Schrodinger, LLC.

Human cell extracts. Lymphoblast and HEK 293T cells were lysed in RIPA buffer (50 mM Tris, pH 8.0, 0.5 M NaCl, 1% NP40, 1% deoxycholate, 0.1% SDS, 2 mM EDTA) with protease inhibitor cocktail (Complete Mini, Roche). Lysates were applied to 12% gels (Invitrogen) or 16% gels (Abcam), transferred to Immobilon-FL (Millipore), and immunoblotted with rabbit anti-RING1A (clone D2P4D, Cell Signaling, #13069, 1:1000), rabbit anti-RNF2 (GeneTex, GTX54707, 1:1000), rabbit anti-HPRT (Santa Cruz Biotechnology, sc-20975, 1:200), mouse anti-histone H2A (clone L88A6, Cell Signaling, #3636, 1:2000) or rabbit anti-$H2Aub_1$ (clone D27C4, Cell Signaling, #8240, 1:2000).

***C. elegans* strains**. *C. elegans* strains were maintained at room temperature (22-24°C) using standard methods (6). N2 (Bristol isolate) was used as the wild-type reference strain. The following strains were used or generated in this work: EG7834: *oxTi415[Peft-3:mCherry:tbb-2UTR]; unc-119(ed3)* (7), PY1058: *oyIs14[P_{sra-6}::GFP, lin-15(+)]*;*lin-15B&lin-15A(n765)* (8), SBP65: *oyIs14[P_{sra-6}::GFP, lin-15(+)]; spat-3(mgw14)*, SBP67: *spat-3(mgw14)*, SBP69: *zdIs13[P_{tph-1}::GFP]* (9), SBP74: *spat-3(mgw26)*, SBP78: *zdIs13[P_{tph-1}::GFP]; spat-3(mgw14)*, SBP79: *oyIs14[P_{sra-6}::GFP, lin-15(+)]; spat-3(mgw26)*, SBP81: *zdIs13[P_{tph-1}::GFP]; spat-3(mgw26)*, VC31: *spat-3(gk22)*. Some strains were provided by the *Caenorhabditis* Genetics Center, which is funded by NIH Office of Research Infrastructure Programs (P40 OD010440).

CRISPR/Cas9 gene editing. *spat-3(mgw14[R209Q])* and *spat-3(mgw26[KO])* were generated using the *dpy-10(cn64)* co-conversion strategy described by Arribere, et al. (10), with the following modifications. Gibson assembly was used to modify the guide

RNA (gRNA)-encoding plasmid pRB1017 (Addgene #59936) by replacing the gRNA cassette with the gRNA(F+E) cassette from plasmid pJW1219 (Addgene #61250), which has been shown to increase editing efficiency (11), yielding plasmid pSP368. gRNA plasmids for targeting the *spat-3* locus were derived from pSP368 by Q5 mutagenesis (New England Biolabs) (12). Plasmid DNA for injection was isolated with the Purelink HQ Mini Plasmid Purification kit (Invitrogen). The distal gonads of wild-type adults were injected with DNA mixes containing 50 ng/μl Cas9 plasmid (pDD162; Addgene #47549) (12), 25 ng/μl of each gRNA plasmid, and ~600 nM of each donor oligonucleotide (IDT). Individual F1 progeny with Rol or Dpy phenotypes were allowed to lay eggs and then lysed for PCR and screening for the restriction site incorporated into the donor oligonucleotide. Mutations at the *spat-3* locus were verified by sequencing, crossed or segregated away from the *dpy-10* marker mutations, and homozygosed.

Microscopy. Worms were mounted on 2% agarose pads and anesthetized with 50 mM sodium azide. Images were obtained using a Nikon 80i wide-field compound microscope.

Histone extraction and analysis. Eggs were isolated from gravid adult hermaphrodites by alkaline hypochlorite treatment and hatched overnight in M9 buffer (13). L1 larvae were collected by centrifugation and stored at -80°. Core histones were isolated with the Histone Purification Mini kit (Active Motif). L1 larvae (0.2-0.4 g) were sonicated in ice cold Extraction Buffer until cuticles were completely broken. Purification was according to manufacturer's instructions except that samples were diluted 2-fold with water after neutralization and Equilibration Buffer was diluted 2-fold with water and used for column equilibration and wash steps. Histone samples were applied to 16% SDS-PAGE gels

(Abcam), transferred to Immobilon-FL membrane (EMD Millipore), and immunoblotted with mouse anti-histone H2A (clone L88A6, Cell Signaling, #3636, 1:2000) or rabbit anti-$H2Aub_1$ (clone D27C4, Cell Signaling, #8240, 1:2000).

SI References

1. Gulsuner S, et al. (2013) Spatial and temporal mapping of *de novo* mutations in schizophrenia to a fetal prefrontal cortical network. *Cell* 154:518-529.

2. Gibson DG, Young L, Chuang RY, Venter JC, Hutchison CA 3rd, Smith HO (2009) Enzymatic assembly of DNA molecules up to several hundred kilobases. *Nat Methods* 6:343-345.

3. Pickart CM, Raasi S (2005) Controlled Synthesis of Polyubiquitin Chains. *Methods Enzymol* 399:21-36.

4. Christensen DE, Brzovic PS, Klevit RE (2007) E2-BRCA1 RING interactions dictate synthesis of mono- or specific polyubiquitin chain linkages. *Nat Struct Mol Biol* 14:941-948.

5. Dhall A, Wei S, Fierz B, Woodcock CL, Lee TH, Chatterjee C (2014) Sumoylated human histone H4 prevents chromatin compaction by inhibiting long-range internucleosomal interactions. *J Biol Chem* 289:33827-33837.

6. Brenner S (1974) The Genetics of *CAENORHABDITIS ELEGANS*. *Genetics* 77:71-94.

7. Frøkjær-Jensen C, Davis MW, Sarov M, Taylor J, Flibotte S, LaBella M, Pozniakovsky A, Moerman DG, Jorgensen EM (2014) Random and targeted transgene insertion in Caenorhabditis elegans using a modified Mos1 transposon. *Nat Methods* 11:529-534.

8. Troemel ER, Kimmel BE, Bargmann CI (1997) Reprogramming chemotaxis responses: sensory neurons define olfactory preferences in *C. elegans*. *Cell* 91:161–169.

9. Sze JY, Victor M, Loer C, Shi Y, Ruvkun G (2000) Food and metabolic signaling defects in a *Caenorhabditis elegans* serotonin-synthesis mutant. *Nature* 403:560–564.

10. Arribere JA, Bell RT, Fu BX, Artiles KL, Hartman PS, Fire AZ (2014) Efficient marker-free recovery of custom genetic modifications with CRISPR/Cas9 in Caenorhabditis elegans. *Genetics* 198:837-846.

11. Ward JD (2015) Rapid and precise engineering of the Caenorhabditis elegans genome with lethal mutation co-conversion and inactivation of NHEJ repair. *Genetics* 199:363-377.

12. Dickinson DJ, Ward JD, Reiner DJ, Goldstein B (2013) Engineering the Caenorhabditis elegans genome using Cas9-triggered homologous recombination. *Nat Methods* 10:1028-1034.

13. Stiernagle, T (2006) Maintenance of *C. elegans*. *WormBook* (ed. The *C. elegans* Research Community), *WormBook* doi/10.1895/wormbook.1.101.1, http://www.wormbook.org.

SI Figures

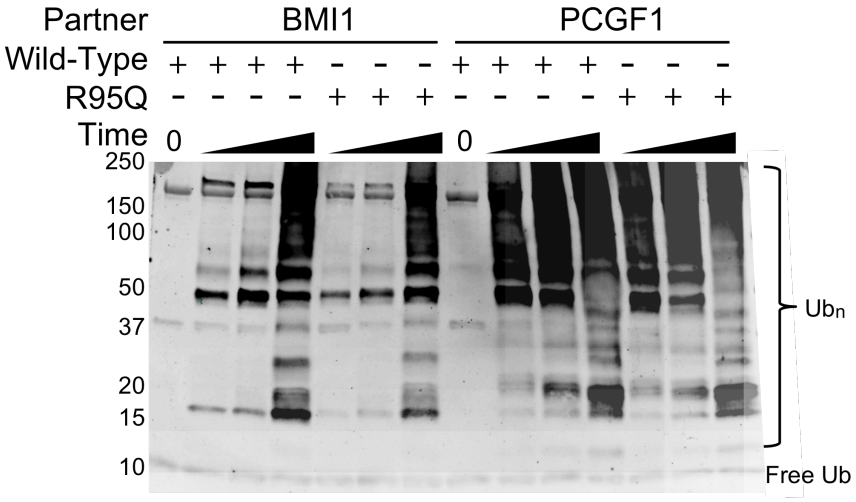

Fig. S1. RING 1 p.R95Q retains ligase activity. *In vitro* ubiquitin-chain building assay of wild-type RING1 or RING1 p.R95Q heterodimers with BMI1 or PCGF1. HA-Ub was detected by immunoblotting of samples taken at 0, 2, 4, and 16 minutes. R95Q does not significantly affect Ub-chain building activity of RING1.

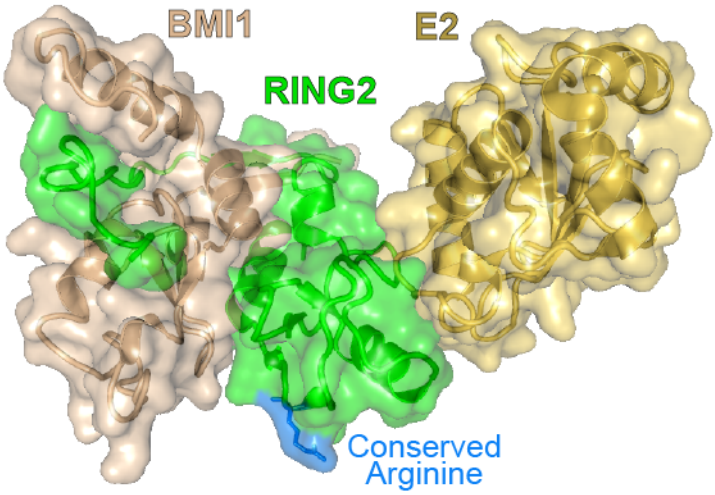

Fig. S2. Structure of RING2/BMI1 RING heterodimer with E2. Structure of BMI1 (tan), RING2 (green), and E2 (gold) (PDB ID=4R8P). The conserved Arg residue homologous to RING1 R95 (blue) is distant from the heterodimer interface with BMI1 and the interface with the E2.

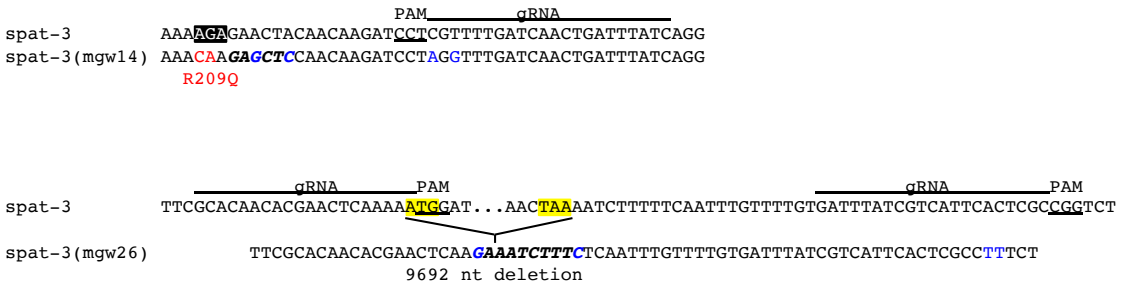

Fig. S3. *spat-3* mutations engineered using CRISPR/Cas9. Schematics of the coding strand of the *spat-3* locus showing the CRISPR/Cas9 editing strategy for the *spat-3(mgw14[R209Q])* and *spat-2 (mgw26[KO])* mutations. The R209 codon is highlighted in black with the coding mutation indicated in red and silent mutations in blue. The *spat-3* start and stop codons are highlighted in yellow, with intervening sequence indicated by a dotted line. gRNA sequences are indicated by a line above the sequence and PAM sequences are underlined. Restriction sites for genotyping are in bold italics.

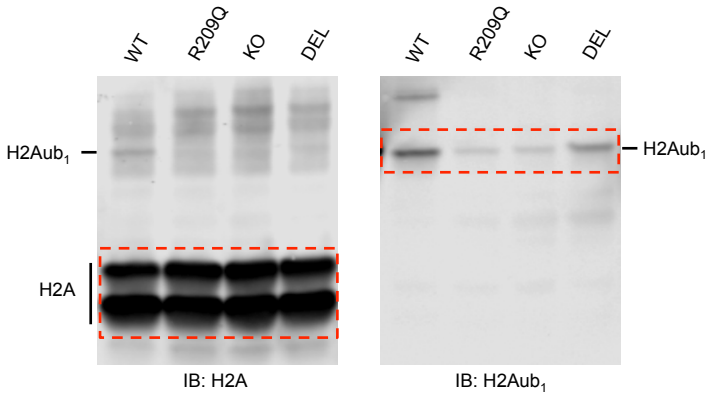

Fig. S4. Uncropped western blots – related to Figure 5. Immunoblot analysis of acid-extracted histones from wild-type larvae (WT) or larvae carrying the SPAT-3(R209Q), knockout (KO) or partial deletion (DEL) mutations. The same blot was probed with anti-H2A (left panel) and anti-H2Aub$_1$ (right panel). Dashed red lines indicate the cropped regions shown in Fig. 5.